Electron tunneling through a planar single barrier in HgTe quantum wells with inverted band structures

L. B. Zhang,[1] Feng Zhai,[2] and Kai Chang[1]
[1]*SKLSM, Institute of Semiconductors, Chinese Academy of Sciences, P.O. Box 912, Beijing 100083, China*
[2]*School of Physics and Optoelectronic Technology and College of Advanced Science and Technology, Dalian University of Technology, Dalian 116024, China*

(Received 24 March 2010; revised manuscript received 10 May 2010; published 21 June 2010)

We present a theoretical study on the electron tunneling through a single barrier created in a two-dimensional electron gas (2DEG) and quantum spin Hall (QSH) bar in a HgTe/CdTe quantum well with inverted band structures. For the 2DEG, the transmission shows the Fabry-Pérot resonances for the interband tunneling process and is blocked when the incident energy lies in the bulk gap of the barrier region. For the QSH bar, the transmission gap is reduced to the edge gap caused by the finite size effect. Instead, transmission dips appear due to the interference between the edge states and the bound states originated from the bulk states. Such a Fano-like resonance leads to a sharp dip in the transmission which can be observed experimentally.

DOI: 10.1103/PhysRevB.81.235323 PACS number(s): 72.25.−b, 73.43.Jn, 73.63.−b

I. INTRODUCTION

Topological insulators (TIs) with time reversal symmetry have attracted a rapid growing interest due to their remarkable band structures and electronic properties.[1] A two-dimensional (2D) or three-dimensional (3D) TI material is characterized by gapless and helical edge or surface states within the bulk excitation gap. The number of Dirac points can be used to classify weak and strong TIs.[2–4] The gapless edge (surface) states show a linear Dirac dispersion and are observed experimentally by using the angle resolved photoemission spectroscopy.[5–7] Interestingly, these edge and surface states are spin filtered and robust against nonmagnetic impurity scattering due to the helicity of these states.[8–10]

In a 2D quantum spin Hall (QSH) system, e.g., a HgTe/CdTe quantum well (QW) with inverted band structures, a single pair of helical edge states in the QSH bar is demonstrated experimentally utilizing the quantized conductance when the Fermi energy lies in the bulk gap.[11–13] Such an edge channel transport could be used to construct spintronic devices with improved performance. To this goal, it is highly desirable to achieve an electric control of the electron transport related with the helical edge states. Very recently, a single barrier in HgTe/CdTe QWs has been fabricated by means of voltage gates,[14] which could be used as a building block for the TI-based ballistic circuits.

In this work, we study the electron transport through planar single-barrier structures in the QSH system based on HgTe/CdTe QWs. As will be seen, rich transmission features will show up as the barrier height varies. Fano-like or Fabry-Pérot-like resonances can be observed due to the interference in the barrier region. The minigap of edge states caused by the finite size effect[15] results in a conductance dip at a finite temperature, as observed in a recent experiment in Hall bar[14] and H-bar[16] structures for QSH effect measurements.

The paper is organized as follows. In Sec. II, we present the model Hamiltonian for the 2D electron gas (2DEG) in HgTe/CdTe QWs under an electric modulation. The description of the transmission calculations based on the scattering matrix method is given for both the full 2D and quasi-one-dimensional (Q1D) cases. In Sec. III, we show the transmission and conductance features of both the full 2D and Q1D systems to illustrate the role of edge states in the tunneling transport. The numerical results are compared with a recent experiment. We make conclusion remarks in Sec. IV.

II. THEORETICAL MODEL

We consider a 2DEG and a QSH bar in the HgTe/CdTe quantum well with inverted band structures, which are schematically shown in Figs. 1(a) and 1(b), respectively. A voltage gate is placed on top of the heterostructure to create an electrostatic modulation $U(x,y)$. For simplicity, the electric

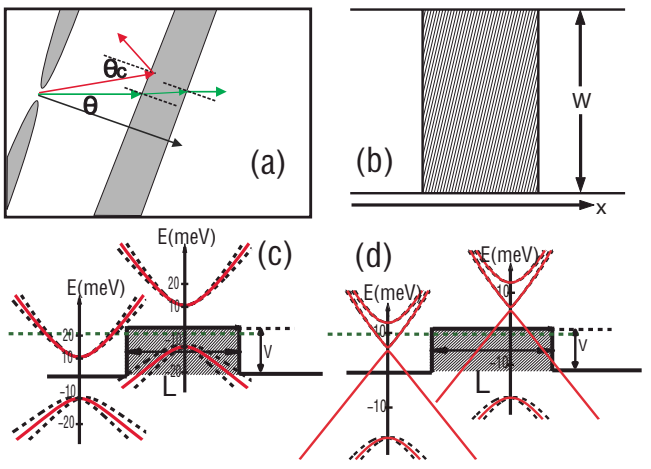

FIG. 1. (Color online) (a)-(b) Schematic illustration of a single-barrier structure based on a 2DEG (a) or Q1D Hall bar (b) confined in a HgTe/CdTe QW with inverted band structures. A rectangular shape with height V and length L is taken for the electric potential. The barrier height can be tuned by a voltage gate on top of the heterostructure. (c)-(d) The energy spectra in the lead and the barrier regions for the considered 2DEG [(c)] and Q1D Hall bar [(d)] systems. The dashed and solid lines correspond to the cases with and without the RSOI, respectively. The green dashed line indicates the position of the Fermi energy E_F.

potential is assumed to be of a steplike, which is V in the stripe region $0<x<L$ and 0 otherwise. The barrier height V can be tuned by adjusting the top gate voltage. Electrons injected from a quantum point contact (QPC) can transmit or reflected by the single electric planar barrier. In a QSH bar [see Fig. 1(b)], there is a lateral confinement imposed on the 2DEG in a HgTe QW. Both systems can be divided into three regions: the left lead region (L), the middle barrier region (M), and the right lead region (R). The comparison between the transport properties of the two systems will reveal the role of the helical edge states in the tunneling through a single barrier.

The low-energy spectrum of carriers in HgTe/CdTe QWs with inverted band structures can be well described by a four-band Hamiltonian, which is obtained from the eight-band Kane model by neglecting the light-hole and spin-split bands.[12] Allowing for the presence of the Rashba spin-orbit interaction (RSOI), such a single-particle Hamiltonian reads

$$H = \begin{pmatrix} H(k) & H_{RSOI}(k) \\ H^*_{RSOI}(-k) & H^*(-k) \end{pmatrix} = \begin{pmatrix} \epsilon_k + M(k) & Ak_- & i\alpha k_- & 0 \\ Ak_+ & \epsilon_k - M(k) & 0 & 0 \\ -i\alpha k_+ & 0 & \epsilon_k + M(k) & -Ak_+ \\ 0 & 0 & -Ak_- & \epsilon_k - M(k) \end{pmatrix}, \tag{1}$$

where $\mathbf{k}=(k_x,k_y)$ is the in-plane momentum of electrons, $H(k)=\epsilon_k I_{2\times 2}+\mathbf{d}(k)\cdot\sigma$, $\mathbf{d}(k)=[Ak_x,Ak_y,M(k)]$ and $\sigma=(\sigma_x,\sigma_y,\sigma_z)$, $\epsilon_k=C+U-D(k_x^2+k_y^2)$, $M(k)=M-B(k_x^2+k_y^2)$, $k_\pm=k_x\pm ik_y$, α is the RSOI strength, and A, B, C, D, and M are the parameters describing the band structure of the HgTe/CdTe QW. Note that the QSH and band insulator are characterized by the sign of the parameter M, which is determined by the thickness of the HgTe/CdTe QW.[12] The velocity operator along the propagating direction, i.e., the x axis, is given by

$$v_x = \begin{pmatrix} -2D_+k_x & A & i\alpha & 0 \\ A & -2D_-k_x & 0 & 0 \\ -i\alpha & 0 & -2D_+k_x & -A \\ 0 & 0 & -A & -2D_-k_x \end{pmatrix}, \tag{2}$$

where $D_\pm=D\pm B$.

The first structure [see Fig. 1(a)] is homogeneous along the y direction. The transverse wave vector k_y is thus conserved. For a given energy E, the plane-wave-like or evanescent-wave-like eigensolutions of the Hamiltonian Eq. (1), in a given region λ ($\lambda=L,M,R$), have the form

$$\psi^\lambda(x,y) = \chi^\lambda \exp[i(k_x^\lambda x + k_y y)]. \tag{3}$$

The longitudinal wave vector $k_x=k_x^\lambda$ is determined from the equation

$$\left(E-\epsilon_k+\sigma\frac{k\alpha}{2}\right)^2 = \left(M(k)+\sigma\frac{k\alpha}{2}\right)^2 + A^2k^2, \tag{4}$$

where $\sigma=\pm 1$ represents the spin branch, $k=\sqrt{k_x^2+k_y^2}$, and $e^{i\theta}=k_+/k$. The analytical expression of the (un-normalized) eigenvector χ^λ is $\{M(k)+E-\epsilon_k, Ake^{i\theta}, [M(k)+E-\epsilon_k]\sigma e^{i\theta}, -\sigma Ak\}^T$.

For the Q1D system shown in Fig. 1(b), the traveling-wave-like or evanescent-wave-like eigensolutions of the Schrödinger equation $H\psi=E\psi$ in a given region λ can be written as the form

$$\psi^\lambda(x,y) = \exp(ik_x^\lambda x)\sum_n \chi_n^\lambda \varphi_n(y), \tag{5}$$

where $\varphi_n(y)=\sqrt{\frac{2}{W}}\sin\frac{n\pi y}{W}$ with $n=1,2,3,\ldots$. The longitudinal wave vector $k_x=k_x^\lambda$ and the eigenvector χ^λ (with 4×1 blocks χ_n^λ, $n=1,2,3,\ldots$) are determined from the following generalized eigenvalue problem:

$$\begin{pmatrix} \mathbf{0} & \mathbf{1} \\ \mathbf{S} & \mathbf{T} \end{pmatrix}\begin{pmatrix} \chi \\ F \end{pmatrix} = k_x \begin{pmatrix} \mathbf{1} & \mathbf{0} \\ \mathbf{0} & \mathbf{X} \end{pmatrix}\begin{pmatrix} \chi \\ F \end{pmatrix}, \tag{6}$$

where $F=k_x\chi$, $\mathbf{S}$, $\mathbf{T}$, and $\mathbf{X}$ consist of 4×4 submatrices with the form

$$\mathbf{S}_{mn} = \begin{pmatrix} \mathbf{\Delta}^+_{mn} & -iA\eta_{mn} & \alpha\eta_{mn} & 0 \\ iA\eta_{mn} & \mathbf{\Delta}^-_{mn} & 0 & 0 \\ \alpha\eta_{mn} & 0 & \mathbf{\Delta}^+_{mn} & -iA\eta_{mn} \\ 0 & 0 & iA\eta_{mn} & \mathbf{\Delta}^-_{mn} \end{pmatrix}, \tag{7}$$

$$\mathbf{T}_{mn} = \begin{pmatrix} 0 & A & i\alpha & 0 \\ A & 0 & 0 & 0 \\ -i\alpha & 0 & 0 & -A \\ 0 & 0 & -A & 0 \end{pmatrix}, \tag{8}$$

$$\mathbf{X}_{mn} = \begin{pmatrix} D_+ & 0 & 0 & 0 \\ 0 & D_- & 0 & 0 \\ 0 & 0 & D_+ & 0 \\ 0 & 0 & 0 & D_- \end{pmatrix}, \tag{9}$$

and $\mathbf{\Delta}^+_{mn}$, $\mathbf{\Delta}^-_{mn}$ and η_{mn} are given by

$$\mathbf{\Delta}^\pm_{mn} = C+U-E\pm M - D_\pm\langle\varphi_m(y)|k_y^2|\varphi_n(y)\rangle, \tag{10}$$

$$\eta_{mn} = \langle\varphi_m(y)|k_y|\varphi_n(y)\rangle. \tag{11}$$

For a given solution ψ^λ with a real k_x^λ, the propagating direction is determined by the sign of its averaged velocity $v^\lambda=\int_0^W \psi^{\lambda+}v_x\psi^\lambda dy=\Sigma_n\chi_n^{\lambda+}v_x(k_x^\lambda)\chi_n^\lambda$, where $v_x(k_x^\lambda)$ is obtained from Eq. (2) by the replacement $k_x\to k_x^\lambda$.

For both systems, we denote the eigenstates [in either the form Eq. (3) or Eq. (5)] $\psi^\lambda_{m;F}$ and $\psi^\lambda_{m;B}$ when it is the mth propagating or evanescent mode along the forward and backward directions. For an electron incident from a given state $\psi^L_{n;F}$ in the left side, the wave functions in the different regions of the structure can be written as

$$\psi_L(x,y) = \psi^L_{n;F}(x,y) + \sum_m r_{m;n}\psi^L_{m;B}(x,y); \quad (12)$$

$$\psi_M(x,y) = \sum_m [c_{m;n}\psi^M_{m;F}(x,y) + d_{m;n}\psi^M_{m;B}(x,y)]; \quad (13)$$

$$\psi_R(x,y) = \sum_m t_{m;n}\psi^R_{m;F}(x,y). \quad (14)$$

The transmission and reflection amplitudes ($t_{m;n}$ and $r_{m;n}$) together with the coefficients $c_{m;n}$ and $d_{m;n}$ are obtained by matching the wave functions and the currents at the two interfaces, which requires $\psi_L(x=0,y)=\psi_M(x=0,y)$, $v_x\psi_L(x=0,y)=v_x\psi_M(x=0,y)$, $\psi_M(x=L,y)=\psi_R(x=L,y)$, and $v_x\psi_M(x=L,y)=v_x\psi_R(x=L,y)$. For the 2DEG system shown in Fig. 1(a), the analytical results of the transmission and reflection are obtained, but omitted here because their lengthy expressions. By means of the scattering matrix theory,[17] we can get the total transmission

$$T = \sum_{m,n}^{RM} \frac{v^R_{n;F}}{v^L_{m;F}} |t_{m;n}|^2, \quad (15)$$

where RM denotes that the sum is taken over all right-moving modes in the left and right side/lead. For a given Fermi energy E_F, the conductance at zero temperature is given by[18]

$$G^0_{QSH}(E_F) = G_0 T(E_F)$$

and

$$G^0_{2D}(E_F) = \frac{W}{2\pi} G_0 \int T(E_F,k_y)dk_y,$$

for the QSH and 2DEG system, respectively, where $G_0 = e^2/h$. At a finite temperature T_B, the ballistic conductance can be written as

$$G(E_F,T_B) = \int \left(-\frac{\partial f}{\partial E}\right) G^0(E)dE, \quad (16)$$

where $f(E)=\{1+\exp[(E-E_F)/(\mathcal{K}_B T_B)]\}^{-1}$ is the Fermi-Dirac distribution.

III. RESULTS AND DISCUSSIONS

We first consider the single barrier based on a 2DEG in a HgTe/CdTe QW with the inverted band structures but without RSOI. The transmission spectra for electrons traversing such a system are shown in Fig. 2, which can be understood from the energy spectra in Fig. 1(c). By tuning the gate voltage, or equivalently, the barrier height V, three tunneling processes can be realized [see Fig. 2(c)]: the intraband process, the interband process, and the tunneling process through the bulk gap. For the case of intraband process, the total transmission shows a slight oscillation around the perfect transmission [see Fig. 2(a) and the black line in Fig. 2(b)]. For the tunneling process occurring between the conduction and valence bands, i.e., the interband tunneling, the Fabry-Pérot resonances are observed due to the multiple reflections in the barrier region between the two interfaces [see the blue lines in Figs. 2(b) and 2(d)]. When the incident energy lies within the band gap of the barrier region [see the red line in Fig. 2(b)], the transmission decays exponentially with the barrier length. In this case electrons can transmit through the barrier via the evanescent mode therein, especially for the normal incidence. More detailed features of the transmission are shown in Fig. 2(f).

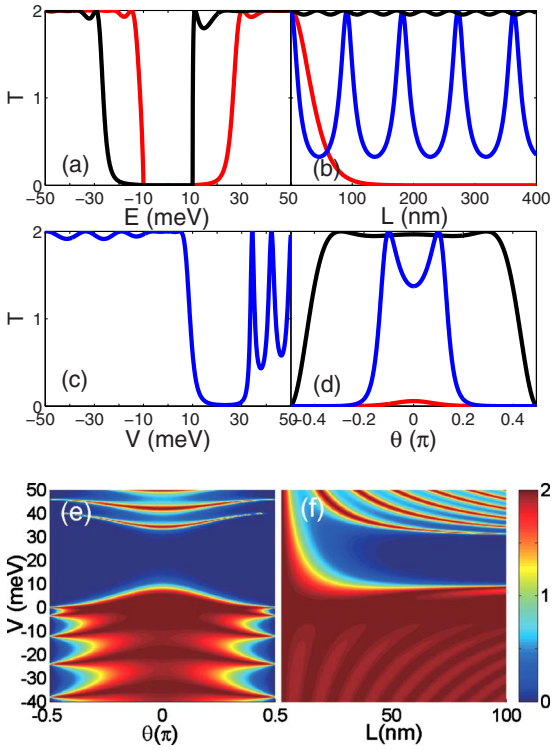

FIG. 2. (Color online) Total transmission T for the single barrier structure based on a HgTe 2DEG. The RSOI is absent. Without special specification, the parameters used in the calculations are $A=364.5$ meV nm, $B=-686$ meV nm^2, $C=0$, $D=-512$ meV nm^2, and $M=-10$ meV. (a)-(d) T is plotted as a function of incident energy E, barrier length L, barrier height V, and incident angle θ. The other parameters in the four panels are: (a) $L=100$ nm, $\theta=0$, $V=-15$ meV (black line) and 15 meV (red line); (b) $E=20$ meV, $\theta=0$, $V=-15$ meV (black line), $V=15$ meV (red line) and $V=35$ meV (blue line); (c) $L=100$ nm, $\theta=0$, $E=20$ meV; (d) $E=20$ meV, $L=100$ nm, $V=-15$ meV (black line), $V=15$ meV (red line) and $V=35$ meV (blue line). (e) Contour plot of T as functions of incident angle θ and potential height V for $E=20$ meV and $L=100$ nm. (f) Contour plot for T as functions of barrier length L and height V for $E=20$ meV and $\theta=0$.

For a fixed incident energy, the transmission is blocked when the incident angle θ is larger than a value θ_C [see Figs. 2(d) and 2(e)]. The critical angle θ_C can be estimated by the Snell's law, $\theta_C \approx \arcsin(k^M/k^L)$, which is accurate for a large barrier length. When the RSOI is included, the transmission resonances will split when interband tunneling occurs (see Fig. 3). The reason is that the Fabry-Pérot interference becomes spin dependent in the presence of RSOI. For the intraband tunneling process, the RSOI would induce a spin splitting for the conduction band, results in the different Fermi wave vectors $k^M_\uparrow$ and $k^M_\downarrow$. One can expect that this spin

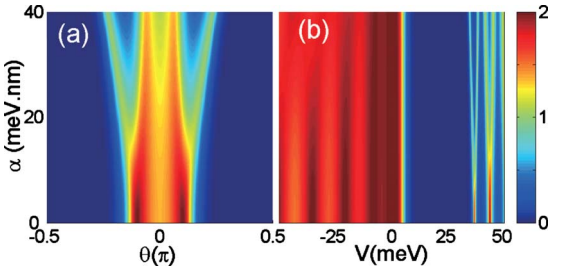

FIG. 3. (Color online) The total transmission T through the single barrier structure in a 2DEG with the RSOI, shown schematically in Fig. 1(a). (a) The contour plot of T as functions of incident angle θ and RSOI strength α for $E=20$ meV, $V=35$ meV and $L=100$ nm. (b) The contour plot for the electron transmission as functions of barrier height V and RSOI strength α for $E=20$ meV, $L=100$ nm and $\theta=0.2\ \pi$.

splitting would lead to different refractions for different spin orientation according to the Snell's law. But the spin splitting is rather small because the Fermi wave vectors $k^M_{\uparrow\downarrow} \approx 0.1 nm^{-1}$ considered in our calculation are quite small. Therefore, the moderate-strength RSOI considered in this work has a slight influence on the transmission [see Fig. 3(b)]. While for the interband tunneling process, the group velocities for electron and hole are very different due to the different effective masses [see Fig. 1(c)]. The RSOI would induce a significant splitting of the resonant peaks in the transmission. These resonant peaks come from the Fabry-Pérot resonances in the barrier region at proper incident angle for a fixed Fermi wave vector in the absence of the RSOI. If the RSOI is included, the Fermi wave vectors of spin-up and spin-down hole states become obviously different for the valence band [see the black dashed line in Fig. 1(c)]. This significant difference would lead to the large splitting of the resonant peaks of the transmission. The similar feature can also be found for the inter- and intra-band tunneling processes at a fixed incident angle by adjusting the gate voltage [see Fig. 3(b)].

So far, we have studied the tunneling of electrons through a single planar barrier in the HgTe 2DEG without the edge effect. Considering a realistic sample with finite transverse size, such as a QSH bar, the effect of the sample edges should be considered in the calculation. For a finite stripe geometry as in Fig. 1(b), the band structures in the barrier and lead region are shown in Fig. 1(d). It can be seen that edge states with a Dirac-like linear dispersion appear within the bulk gap. A tiny gap for the edge states can be discerned in Fig. 1(d) due to the effect of a finite transverse size. Hereafter we focus mainly on the electron transport process concerning edge channels. In Q1D QSH bar, the RSOI has a minor influence on the total transmission. This is because the Rashba spin-orbit interaction arising from the structure inversion asymmetry will coupled the spin-up and spin-down subbands at the same in-plane momentum k. For the edge states, the spin-up and spin-down electrons with the same in-plane momentum localize at the opposite edges, the overlap of their wave functions can be negligibly small, therefore the RSOI would not affect the edge states significantly.

In Figs. 4 and 5, we show the transmission variations with the barrier height, the incident energy, and the structural pa-

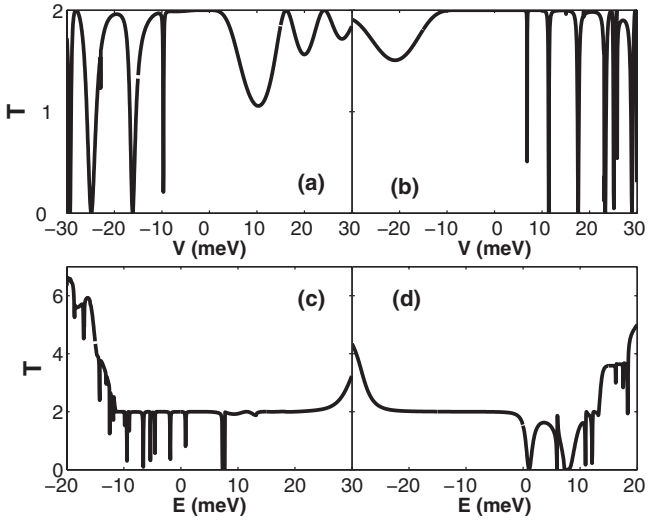

FIG. 4. The total transmission T through a single barrier in a QSH bar [see Fig. 1(b)]. (a)-(b) The transmission T as a function of barrier height V for $E=10$ meV (a) and -10 meV (b). (c)-(d) The transmission T as a function of incident energy E for $V=15$ meV (c) and $V=-15$ meV (d). The barrier length and the wire width are taken as $L=100$ nm and $W=200$ nm, respectively.

rameters for a Q1D QSH bar with width $W=200$ nm. When the incident energy E is fixed at a value in the bulk gap but not in the edge gap of the leads, several tunneling processes will happen as the barrier height V changes [see Figs. 4(a), 4(b), 5(a), and 5(d)]. If the incident energy E locates in the bulk gap of the barrier region and in the same or opposite branch of the linear spectrum, the transmission is nearly perfect or oscillating with V. The oscillation also originates from the Fabry-Pérot interference since the velocities of edge states in up branches are slightly different especially at the Fermi energy $E_F > 20$ meV, although the energy spectrum of the edge states seems perfectly linear [see Fig. 1(d)]. For the special case that incident energy E is in the edge gap of the barrier region, the transmission decays exponentially with the barrier length [see Figs. 5(a) and 5(d)] due to the absence of a propagating mode in the barrier region. The most interesting feature is observed as the incident energy E is close to the bottom or top of a sub-band of bulk states. In this case, electrons can either propagate via edge channels through the barrier region or tunnel through the same region via quasibound states derived from this sub-band. The interference between the propagating edge states and the evanescent states leads to a series of Fano resonances in the transmission spectrum. Sharp transmission dips also appear if incident energy E is outside the bulk gap of the leads but within that of the barrier region [see Figs. 4(c) and 4(d)]. The transmission features presented above depend strongly on the energies of the quasibound states confined in the barrier, which can be tuned by the gate voltage as well as the structural parameters (L and W). This is clearly reflected in Fig. 5. Here, it should be stressed that the perfect transmission is a unique feature that the electron transport in a Q1D TI bar via the topological edge states. This can be observed easily in Figs. 4(a)–4(d), 5(a), 5(b), 5(d), and 5(e), e.g., the region at $10 < E_F < 25$ in Fig. 4(c), $-25 < E_F < 0$ in Fig. 4(d) and especially at the re-

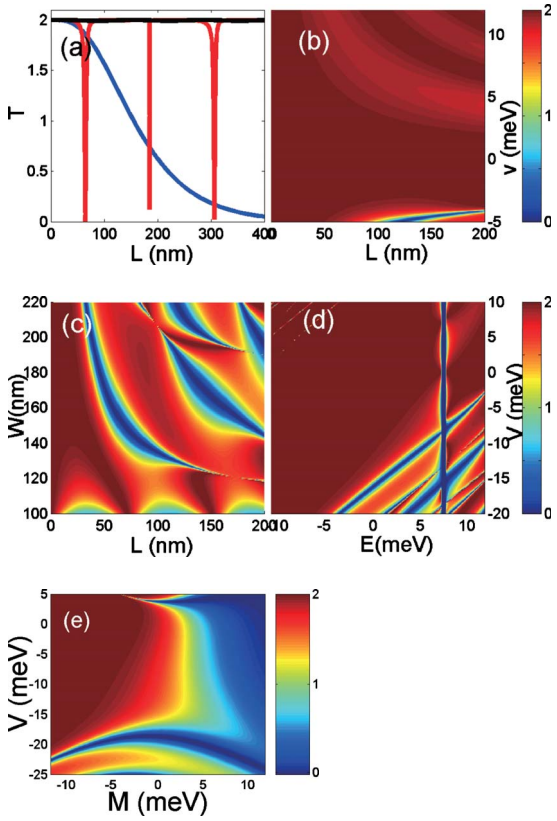

FIG. 5. (Color online) The total transmission T through a single barrier in a Q1D QSH bar. (a) The dependence of T on the barrier Length L. The wire width is $W=200$ nm and the incident energy is set at $E=13$ meV. The potential height is set at $V=5$ (black line), -5 (red) line, and 5.5 (blue line) meV. Note that the blue line corresponds to the tunneling through the gap in the barrier region. (b) Contour plot of T as functions of L and V for $E=10$ meV and $W=200$ nm. (c) Contour plot of T as functions of L and W for $E=10$ meV and $V=-10$ meV. (d) Contour plot of T as functions of E and V for $L=100$ nm and $W=200$ nm. (e) Contour plot of T as functions of M and V for $L=100$ nm, $W=200$ nm and $E=-5$ meV.

gion $M<0$ in Fig. 5(e) where the electron transmits through the barrier nearly perfectly. But for the case that the electron transport in a Q1D band insulator bar [see Fig. 5(e) at the region $M>0$], this conductance plateau disappears. This clearly demonstrates that there is a big difference in the conductances for the topological insulator ($M<0$) and band insulator ($M>0$) spin Hall bars.

Finally we examine to what extent the transmission features shown above are reflected in the measurable quantity, the conductance G at a finite temperature. In Figs. 6 and 7 the conductance at $T_B=4$ K are plotted as a function of $V_g=-V$ for both the 2DEG and QSH system. For comparison the zero-temperature conductance G^0 is also presented. For the 2DEG system, the profile of the conductance curve is almost unchanged by the temperature-induced average effect, where the conductance curves can be calculated by intergration over all the incident angles. At $T_B=4$ K the zero-conductance region shrinks. For the QSH system the Fermi energy is fixed at such a value that several bulk sub-bands in

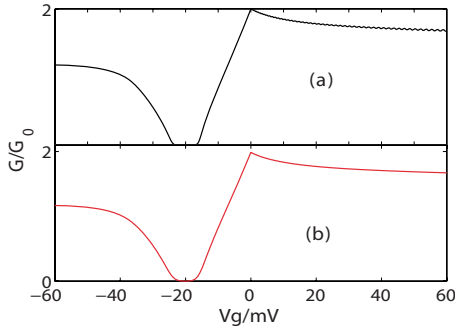

FIG. 6. (Color online) (a) The dependence of the conductance G on $V_g=-V$ for the single barrier structure based on a HgTe 2DEG at zero temperature. The barrier length $L=1000$ nm, the Fermi energy $E_F=20$ meV and $M=-4$ meV. (b) Same as (a), but at a finite temperature $T_B=4$ K.

the leads are open. With the variation of V_g, the number of propagating channels in the barrier region changes which determines the height of conductance plateau shown in Fig. 7(a). The rapid oscillations appear in the G^0-V_g curve due to the presence of Fano resonances and multimode interferences. Note that in the given parameters the gap of edge states is approximately 3 meV and thus a remarkable conductance gap is seen. At $T_B=4$ K the interference effect is washed out and the conductance gap becomes a valley [see Fig. 7(b)]. The presence of a conductance valley rather than a conductance gap [as in Fig. 6(b)] in the $G-V_g$ curve agrees well with a recent conductance measurement.[14] On the two sides of the conductance valley, a perfect plateau with height $2e^2/h$ appears due to the contribution of the edge channels. The width of the conductance plateau and the gap are sensitive to the system parameters (particularly, the parameter M) which can be controlled by the thickness of the HgTe QW. In Fig. 7(b) the conductance decays in the high V_g regime, while a saturation has been observed in the experiment. This reason for this difference is that the light-hole band neglected in the four-band model provides additional transport channel.

IV. CONCLUSIONS

In summary, we have theoretically investigated the electron tunneling through a planar single barrier in a HgTe/

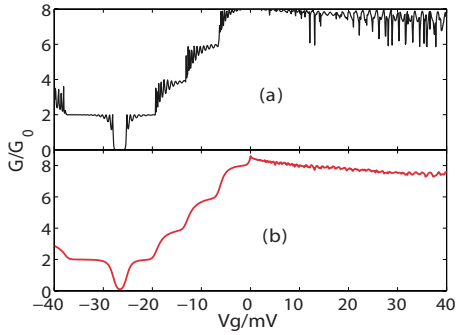

FIG. 7. (Color online) (a) The dependence of the conductance G on $V_g=-V$ for the single barrier structure based on a Q1D QSH bar at zero temperature. The parameters are $W=200$ nm, $L=1000$ nm, $M=-4$ meV, and $E_F=30$ meV. (b) Same as (a), but at a finite temperature $T_B=4$ K.

CdTe quantum well with inverted band structures in 2DEG and Q1D systems. We have shown that in a 2DEG system the electron transmission exhibits a series of peaks for the interband tunneling process, which comes from the quantum interference of electron propagating forth and back in the barrier region. For the interband tunneling process, the transmission of electrons shows a strong dependence on the strength of RSOI, due to the lifting of the spin degeneracy of the energy bands, and the resonant peaks split into the doublet. In Q1D system, for the QSH-bar, it displays a series of Fano dips for the intraband tunneling process and a slightly oscillation for the interband tunneling process. These tunneling processes are dependent on the quasibound states strongly, e.g., the Fabry-Pérot modes, in the barrier. These resonance are highly sensitive to the temperature effect.

ACKNOWLEDGMENTS

This work was supported by the NSFC (Grant Nos. 60525405, 10874175, and 10704013) and RFDP (Grant No. 200801411042), and the bilateral project between Sweden and China.

[1] X. L. Qi and S. C. Zhang, Phys. Today **63**(1), 33 (2010).
[2] L. Fu, C. L. Kane, and E. J. Mele, Phys. Rev. Lett. **98**, 106803 (2007).
[3] L. Fu and C. L. Kane, Phys. Rev. B **76**, 045302 (2007).
[4] J. E. Moore and L. Balents, Phys. Rev. B **75**, 121306(R) (2007).
[5] D. Hsieh, D. Qian, L. Wray, Y. Xia, Y. S. Hor, R. J. Cava, and M. Z. Hasan, Nature (London) **452**, 970 (2008).
[6] Y. Xia, D. Qian, D. Hsieh, L. Wray, A. Pal, H. Lin, A. Bansil, D. Grauer, Y. S. Hor, R. J. Cava, and M. Z. Hasan, Nat. Phys. **5**, 398 (2009).
[7] X. L. Qi, T. L. Hughes, and S. C. Zhang, Phys. Rev. B **78**, 195424 (2008); X. L. Qi, R. Li, J. Zang, and S.-C. Zhang, Science **323**, 1184 (2009).
[8] C. L. Kane and E. J. Mele, Phys. Rev. Lett. **95**, 146802 (2005).
[9] C. Xu and J. E. Moore, Phys. Rev. B **73**, 045322 (2006).
[10] C. J. Wu, B. A. Bernevig, and S. C. Zhang, Phys. Rev. Lett. **96**, 106401 (2006).
[11] C. L. Kane and E. J. Mele, Phys. Rev. Lett. **95**, 226801 (2005); B. A. Bernevig and S. C. Zhang, *ibid.* **96**, 106802 (2006).
[12] B. A. Bernevig, T. L. Hughes, and S. C. Zhang, Science **314**, 1757 (2006).
[13] M. König, S. Wiedmann, C. Brune, A. Roth, H. Buhmann, L. W. Molenkamp, X. L. Qi, and S. C. Zhang, Science **318**, 766 (2007).
[14] H. Buhmann and L. W. Molenkamp private communication.
[15] B. Zhou, H. Z. Lu, R. L. Chu, S. Q. Shen, and Q. Niu, Phys. Rev. Lett. **101**, 246807 (2008).
[16] C. Brüne1, A. Roth, E. G. Novik, M. König, H. Buhmann, E. M. Hankiewicz, W. Hanke, J. Sinova, and L. W. Molenkamp, Nat. Phys. **6**, 448 (2010).
[17] Lebo Zhang, P. Brusheim, and H. Q. Xu, Phys. Rev. B **72**, 045347 (2005).
[18] S. Datta, *Electronic Transport in Mesoscopic Systems* (Cambridge University Press, Cambridge, England, 1995).